Analysis of Liquid Column Instabilities of a Plain Liquid Jet in a Crossflow Using Image Processing Techniques

Q. Wang, U.M. Mondragon, C.T. Brown*, and V.G. McDonell
Energy Research Consultants
23342 South Pointe Drive, Suite E
Laguna Hills, CA 92653-1422

Abstract

The injection of a plain liquid jet into a gaseous crossflow has been studied extensively. Numerous empirical models describing the aspects of the breakup, penetration and dispersion of the liquid jet have been developed based on the experimental data obtained. In recent years, however, more advanced models for the jet breakup process are being developed. As these more sophisticated simulation approaches such as surface tracking methods evolve, a richer database for assessing accuracy is of great interest. In parallel, advancements in imaging diagnostics for capturing details regarding the breakup processes have also evolved, creating an opportunity to provide new types of results that can be used for model validation. While these imaging methods are convenient to apply, extraction of the necessary quantitative information to compare directly with advanced simulation methods requires considerable effort. Due to the vast amounts of data that can be generated in a matter of seconds, manual analysis of the images obtained can be tedious. As a result, automated methodologies for extracting this information are necessary. To this end, the present work describes the development of automated processing routines and their application to the breakup of a plain liquid jet in a crossflow under varying conditions. Examples are given in the form of expressions for column breakpoint time and trajectory based on thousands of images from a wide range of conditions. In the present paper, emphasis is given to analysis of the dynamic nature of the breakup and liquid column characteristics such as variation in breakpoint location and identification of dominant frequencies. The results are correlated with appropriate non-dimensional groups and expressions describing these dynamic characteristics are provided.

*Corresponding author

Background and Objective

The modeling of liquid jet injection into a gaseous cross flow has been progressively studied beginning with prediction of an averaged far field spray characteristics and building up to predictions of more complex phenomena relating to the near field and the liquid column [1,2,3,4]. With increasing modeling focus on the liquid column, new measurement systems and analysis are required to produce data sets for model development and validation.

Recently, high speed video has become a common data acquisition system for recording the behavior of the liquid column, but often the processing of these video yields only interpreted or qualitative results. To address this shortcoming, automated quantitative processing software tools are of increasing interest. In the present work automated tools have been developed and applied to the analysis of the liquid column (1) break point and time, (2) trajectory, and (3) instabilities. This work extends previous efforts directed at the first two characteristics [5].

For jets in a cross flow, the break time of the liquid column is usually chosen as a primary characteristic over other possible choices such as the length or stream-wise location of the break point for a few reasons. For example, liquid column break time has a physical relationship with the experimental parameters treated in the current study including air velocity, liquid velocity, and orifice diameter. Also the break time is an important value for modeling purposes in the liquid jet in crossflow [4,6]. Besides, the break time remains on the same scale throughout the entire range of practical operating conditions. In addition, break times remain continuous throughout the three breakup modes: column, multi-mode, and column shear.

Liquid column trajectory is also of interest because of (1) its relationship to liquid column break time and (2) its effect on important spray characteristics such as penetration and liquid mass distribution downstream.

However, the breakup time and liquid column trajectory are generally described in terms of "static" quantities based on specific conditions. The reason is that the majority of the breakup time and liquid column trajectory expressions are based on information extracted from single images. Hence they are based on static images and thus do not contain any 'dynamic' information. Often several stills from a given condition are used to generate averaged information to improve accuracy, but this does not capture the time resolved dynamic information associated with the breakup process (e.g., the frequency associated the liquid column breakup).

One way to extract the instability information of the liquid column is to apply frequency analysis (FFT, for example) on the static data such as breakpoint location and liquid column trajectory and extract the major frequency of the instability.

Figure 1 shows the overlapped locations of the breakpoints of liquid columns from about 100 frames, which are color coded with time. As shown in Figure 1, the locations of the liquid column breakpoints vary significantly, yet in an ordered manner over the sequence of images for a fixed experimental condition. The major frequency f of the temporal fluctuation of these breakpoints is considered to reflect dynamics of the jet in cross flow and can be used to characterize it. The Strouhal number, St, which is defined in Eq. 1 and based on the instability frequency f and the jet diameter d, is believed to closely match the value obtained from the vortex shedding of a cylinder with the same diameter [7]. It has been shown that St is usually equal to 0.15 for $2 < r < 8$, where r is the effective velocity ratio and defined as the square root the momentum flux ratio q as shown in Equs. 2 and 3.

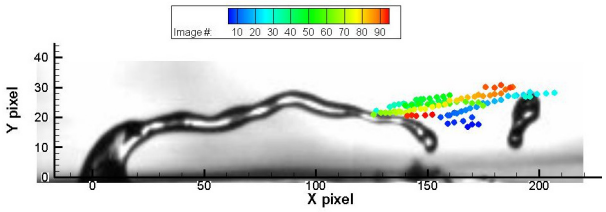

Figure 1. Liquid column breakpoint spatial distribution

$$St = \frac{f d_j}{U_j} \tag{1}$$

$$r = \sqrt{q} = \sqrt{\frac{\rho_j U_j^2}{\rho_c U_c^2}} \tag{2}$$

$$q = \frac{\rho_j U_j^2}{\rho_c U_c^2} \tag{3}$$

The frequency information of the liquid column will be useful for many applications. For example, this frequency associated with the liquid column breakup may play an important role in other phenomena such as combustion instability [8]. Also the frequency data extracted from the video can be used to validate the CFD simulation results which require frequency information of the liquid jets, such as the Large Eddy Simulation (LES) of the jet in cross flows [9].

According to Eq. 1, the instability frequency f of the liquid column should depend on the liquid jet properties (jet velocity U_j and jet diameter d_j) and have little dependency on cross air flow properties as long as $2 < r$

< 8. To verify this conclusion, *f* is correlated with these two parameters in the analyses presented. Additionally, correlations for *f* based on the key physical nondimensional quantities are also developed. The key quanties include (1) the momentum flux ratio as mentioned above as well, (2) the Reynolds number,

$$Re_j = \frac{\rho_j U_j d_j}{\mu_j} \tag{4}$$

(3) the aerodynamic Weber number, (in this case based on the crossflow properties) and (4) the liquid Weber number (based on the liquid properties) :

$$We_c = \frac{\rho_c U_c^2 d_j}{\sigma} \tag{5}$$

$$We_l = \frac{\rho_j U_j^2 d_j}{\sigma} \tag{6}$$

Using these dimensionless groups in the description of the liquid column instable frequency *f* provides a physical basis for interpreting the behavior.

Reynolds number is not featured prominently in many of the general jet behavior correlations. This parameter indicates the presence of instabilities on the jet surface as a transition from laminar to turbulent behavior occurs. Recent studies suggest that once the jet is turbulent, the effect of other parameters such as the crossflow velocity on the nature of the atomization becomes less important [10,11].

The gas Weber number represents the ratio of the aerodynamic forces to the surface tension forces. The crossflow velocity used is typically that of the freestream determined from volumetric flow and test section cross sectional area. Similarly, the liquid Weber number represents the ratio of the liquid inertial forces to the surface tension forces.

The momentum flux ratio represents the relative strength of the liquid jet momentum in the injection direction versus the air momentum in the crossflow direction. For the liquid velocity, the volumetric flow was measured and divided by the orifice area. For the air, the mass flow and temperature were measured. The velocity was then calculated dividing by both the density and test section cross-sectional area. In other words, the discharge coefficient has been assumed to be 1 for purpose of this work.

In addition to the continuous effects of experimental parameters on liquid column breakup, the dominant mode of column breakup changes as the air and liquid flows vary. Typically the breakup process is split up into three regimes: column instability breakup, multimode breakup, and column shear breakup.

The objective of the current work is to present correlation of the liquid column instable frequency based on a few independent variables of the liquid jet and non-dimensional characteristics of possible operating conditions and to describe a methodology to extract liquid column frequency information from high speed video of liquid jet in crossflow experiments in an automated and statistically significant way. The data set analyzed is the same as that used in a previous study to document the near field and liquid column behavior [3,11].

In addition to the correlations resulting from the current work over a wide range of operating conditions and incorporating many of the pertinent operating parameters, the methodology is scalable to large data sets including a more detailed matrix of test conditions and including all of the key variables driving the physical phenomena of liquid column breakup, even though the analysis based on Eq. 1 and the results suggest it is sufficient to correlate the instability frequency using only liquid jet properties.

Approach

The examination of the liquid column breakup analysis resulted in the prediction of liquid column break point location, liquid column trajectory and the instability frequency based on experimental parameters including injector orifice diameter, aerodynamic Weber number, and momentum flux ratio. The details of the experimental methods can be found elsewhere [12], however the key features are briefly described here. High speed video shadowgraphs were acquired to capture the time resolved behavior of the liquid jet injected at 90-deg into a subsonic crossflow. These shadowgraphs were then analyzed to (1) find a mass-averaged trajectory and (2) identify a spatial location of the liquid column break point. After the spatial characteristics for each image were identified, a Fast Fourier Transformation (FFT) process was carried out for the results over entire videos in time domain and the major frequency of the instability was picked up according to the FFT results. Finally, correlation and multivariable linear regression analyses were conducted on the FFT results to associate the instability frequency to the liquid jet properties and other pertinent, non-dimensional parameters of the various experimental conditions. Variations of air velocity, liquid velocity, and orifice diameters were taken into account while the liquid properties used were those of the test fluid used, Mil-PRF-7024-Type II, at 25 deg C.

High speed videos containing at least 200 images were recorded for each of the experimental conditions described in Table 1.

Table 1. List of Experimental Conditions

Case	*Diameter mm*	*We_l **	*We_c **	*Momentum Ratio*
1	0.5	9	117	10
2	0.5	9	620	52
3	1.3	94	124	1
4	1.3	94	262	2
5	1.3	94	445	4
6	1.3	94	714	6
7	1.3	94	1070	9
8	1.3	94	1461	12
9	1.3	94	1911	16
10	1.3	140	475	3
11	1.3	140	749	4
12	1.3	140	1070	6
13	1.3	140	1475	8
14	1.3	140	1899	10
15	1.3	140	2400	13
16	1.3	140	3162	17
17	0.5	314	3204	8
18	0.5	314	5084	13
19	0.5	314	8130	20
20	0.5	314	21999	54
21	0.9	345	436	1
22	0.9	345	1352	3
23	0.9	345	3054	7
24	0.9	345	4845	11
25	0.9	345	8323	19

*We_l is the liquid Weber number and We_c is the aerodynamic Weber number.

Liquid velocity based on volume flow divided by injector physical area

Gas velocity based on volume flow divided by the test section cross section.

Image processing and break point detection were performed on each image (more than 5,000 data points), and the correlation and regression analyses were performed on an average of the values in each of the 25 cases listed.

Experimental Apparatus

Test Section. A test section with inner dimensions of 69.85 mm x 69.85 mm was used for the experimental studies. A 150 mm round to square transition was accomplished over a length of 300 mm. Additional details of the geometry are shown in Figure 2.

The cross flow air velocity (nominally 60 m/s) was established using a blower (Spencer) capable of delivering about 2 lbs/sec at about 3 psig (at the blower outlet). The air flow was metered with a calibrated mass flow meter (Sierra Instruments). The actual test section velocity was checked using a Pitot probe.

The test liquid was supplied by a gear pump capable of delivering about 3.8 l/m about 2,200 kPa. The liquid flow was measured with a calibrated turbine meter (EG&G Model FTO-1 w/extended range) that has a range of 0.038 to 0.3 l/m with accuracy of 0.05% of reading. A pressure transducer (Omega Model PX212-15G) with a 0-100 kPa range w/ 0.25% accuracy was used to log pressure upstream of the injector, but downstream of the shutoff and control valve. A glycerin filled pressure gauge (0-15psig) was used to check the pressure readings.

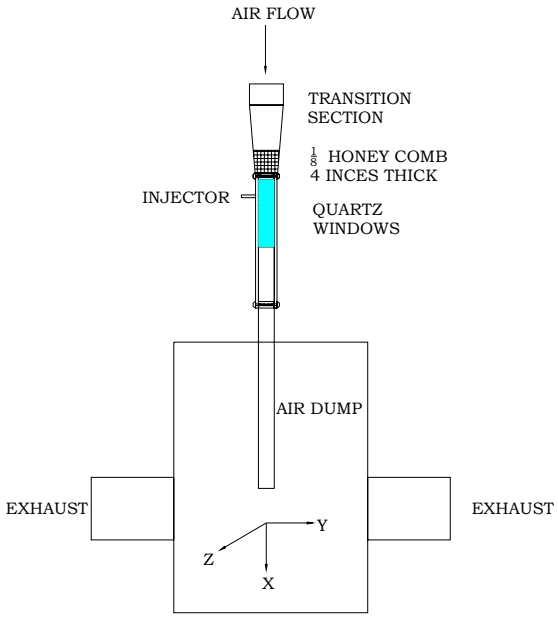

Figure 2. Test Section.

Further details about the experimental apparatus and measurement methodology can be found in previous studies [3,12].

Methodology

The methods used for the image processing and boundary detection, liquid jet trajectory mapping and fitting, break point detection and trajectory error analysis were explained in detail elsewhere [12]. However, the steps are described here briefly for convenience.

Image Preprocessing. To streamline the core of the calculations performed on the videos and to ensure that the program is insensitive to changes in experimental conditions or acquisition procedure, some preprocessing of the images was required.

First, the videos are split into a set of individual tiff images allowing for manipulation by image editing software packages or programming languages. Once the videos have been converted to a usable form, the region upstream of the injection and any other region that does not contain the liquid phase are cropped out. In addition, the images were oriented and adjusted to ensure that cases with differing acquisition and environments are directly comparable. A few techniques to

reduce the background noise of the images are used. Figure 3 shows and example an image before and after preprocessing.

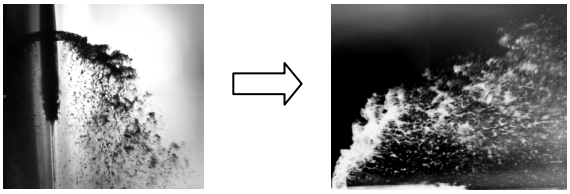

Figure 3. Example of Image Before and After Preprocessing

Liquid Column Trajectory Mapping. The liquid column trajectory serves as a path along which to search for the liquid column break point and serves as a method of locating the break point that is consistent over the range of images in each high speed video and images from one video to the next. Also, by fitting the liquid column trajectory using all of the pixels illuminated by the liquid column and assigning the break point to be an on the trajectory path, the break point location can be assigned in a way that is insensitive to the local liquid column distortions and the non-symmetric behavior of the liquid column typical at breakup. The process of fitting a continuous trajectory to the image of the liquid column is made up of three parts: (1) isolation of liquid column, (2) selection of a fit equation, and (3) regression of the fit coefficients using the Hough transform method.

Pixels signifying the liquid column were selected based on the assumption that the image background, which illuminates most of the pixels can be defined as a random range of illumination centered around the noise floor. This noise floor and the range about the noise floor were designated as the median intensity of the entire image and two standard deviations accordingly. The image was then threshold at the intensity corresponding to the median plus two standard deviations.

The second step, selecting a fit equation was accomplished by first looking to existing studies. Based on these studies [13,14,15] the possibilities were reduced to linear, exponential, and log fit. Previous studies [5] demonstrate that an equation of the form in Equation (7) is the best choice of a fit equation for the liquid column.

$$y = m\ln(x) + y_o \qquad (7)$$

where m and y_o are fitting coefficients.

Fit Process. The standard fitting method for a linearized fit equation such as Equation (7) is the Least Squares method which minimizes the error for all of the data points compared to the fit equation. Although this method is fast and efficient, it is only capable of fitting a single curve to all of the data. Using this method in the current set of data produces a bias towards the wall since a large number of pixels to be fit are intensities generated by the surface reflection and not signal due to the liquid column. Instead the Hough transform method was used to fit the liquid column [16].

The Hough transform is commonly used when identification of more than one object or curve is desired. This feature is exploited to locate both the wall and the liquid column. Then eliminate the wall as a whole rather then eliminating each pixel in the wall reflection, which is a desired feature in this case. Compared to the Least Square fitting method, Hough transformation is much computationally intensive and requires 2-3 minutes to fit one image. The liquid column trajectory fitting result for case 24 using Hough transformation method is show in Figure 4.

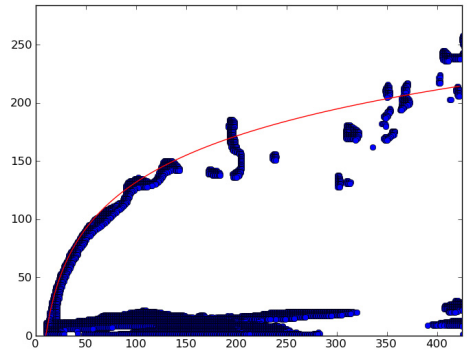

Figure 4. Liquid column trajectory fitting using Hough Transformation method

Trajectory Error Analysis. The liquid column trajectory mapping process has three sources of error. The first is discretization of the measurement region into pixel sensors on the camera giving an uncertainty of 1 pixel in any direction of the position of any feature captured. Discretization also causes the location of the orifice center to also have an uncertainty of 1 pixel because the edge of the liquid column at injection can only be identified to an accuracy of 1 pixel. Finally, the binning of the Hough transform causes the fit slope, m, to have an uncertainty up to 7%. The maximum uncertainty was applied to the maximum break height yielding a value of 1.65 pixels. The position of any point on the liquid column trajectory then has a value of 2.2 pixels arrived at using Equation (8).

$$\varepsilon_{trajectory} = \sqrt{\sum \varepsilon_i^2} \qquad (8)$$

Break Point Assessment. Identifying the break point was completed using a process of 5 steps:

1. Detecting the liquid column and clump boundaries.
2. Stepping along the liquid column trajectory.
3. Defining a slice in space that is normal to the trajectory at that point.
4. Counting the number of boundary pixels within the defined slice.
5. Designating the first point not containing a significant number of boundary pixels.

Boundary Detection. Creating a boundary image was accomplished by scanning through the image at each pixel location and assigning a new value based on the sum of the difference between matching neighboring pixels. Then a binary threshold was performed on the boundary values and saved as a separate image.

Step Along Liquid Column Trajectory. To ensure that each slice was evenly spaced from the beginning of the liquid column where the trajectory is primarily vertical to primarily horizontal near the break point, the position of each ensuing step was calculate using the arc length. The change in the horizontal direction, x, was estimated using a line tangent to the liquid column trajectory. Then the change in x corresponding to the distance of 1 pixel along the tangent line was calculated as follows in Equation (9): Once the new x-location was found, the y value was solved using the liquid column trajectory.

$$dx = \sqrt{1 + \frac{m}{x}} \qquad (9)$$

Breakpoint Detection. After the start point on the liquid column trajectory was established, a slice perpendicular to the trajectory at that point was created. A slice is then constructed of each pixel that falls on a line normal to the trajectory of length one diameter and all of the neighboring pixels. The neighboring pixels were included to ensure that boundaries were not skipped because of rounding from the transformation between the continuous line and discrete pixel locations.

The break point location corresponds to the first empty slice as opposed to the last slice containing boundary pixels. The first empty slice in this case is more indicative of the break point. Because of the overlapping nature of the slices, two or more slices may "see" the same pixel and therefore more than one slice could be counting the last boundary pixel at the breakpoint. Therefore the first empty slice was chosen to identify the break point because it is definitely unique whereas the last slice containing boundary pixels may be ambiguous because some of the pixels may have already been counted. The result of this detection algorithm is shown in Figure 5, which is from the Case 24 in Table 1. The breakpoint is accurately detected at the end of the liquid column trajectory.

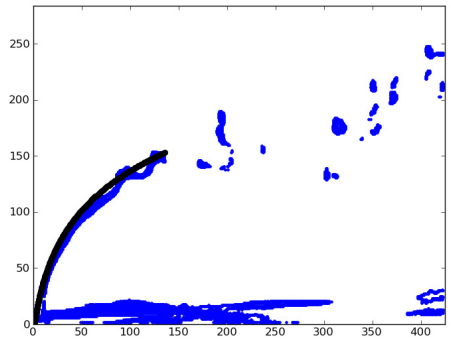

Figure 5. Breakpoint detection

Breakpoint Error Analysis. Two different types of error are inherent to the break point assessment. The first was the qualitative classification of the liquid column break point. Identification of the liquid column break point by visual inspection may be different then the local area that the algorithm identified as the break point. The program was calibration such that the identification of a break point was conservative. In many respects large liquid clumps act in a fashion similar to the liquid column, and so the program is likely to chose a break point that was designed to be longer than what may be identified by visual inspection. This type of error will be ignored as a widely accepted break point definition does not yet exist.

The second type of error is the quantitative errors due to discretization and calculation. The error in the x direction is 1.28 pixels. Once the x break location is found it is used with the trajectory equation to find the y break location. This method yields a maximum error in y of 31.4 pixels. The uncertainty in the y direction is much higher because it is dependant on the x uncertainty and the uncertainty associated with trajectory fit.

Breakpoint Location. Once the breakpoint location is determined by the process above for each frame of the video, the spatial coordinates (x and y values in the image) for it are recorded and saved in a CSV file by the program for further processing.

The temporal change of the x coordinate of the breakpoint is plotted in Figure 6 below. The x direction is defined as the direction in the cross flow direction and y direction is defined as the direction of the liquid jet into the cross flow. It can be seen from Figure 6 that the movement of the breakpoint in x direction has obvious periodicities. Multiple modes and different frequencies associated with the fluctuation can also be observed. It should be noted that the similar trend can be observed for the movement in the y direction.

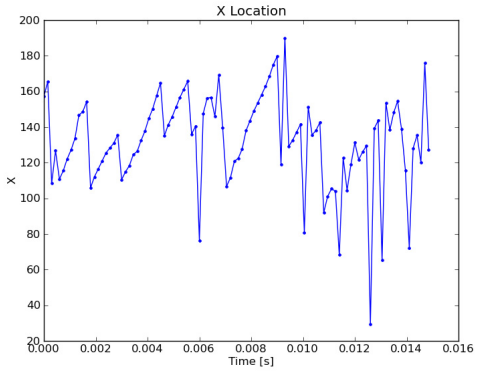

Figure 6. Temporal fluctuation of the breakpoint location in x-direction

Instability Analysis. The location data shown in Figure 6 can be transformed into the frequency domain using FFT and the dominating frequency of the liquid column breakpoint movement can be extracted. The constructed periodogram (power vs frequency) plot from the FFT results of Case 24 is shown in Figure 7 .

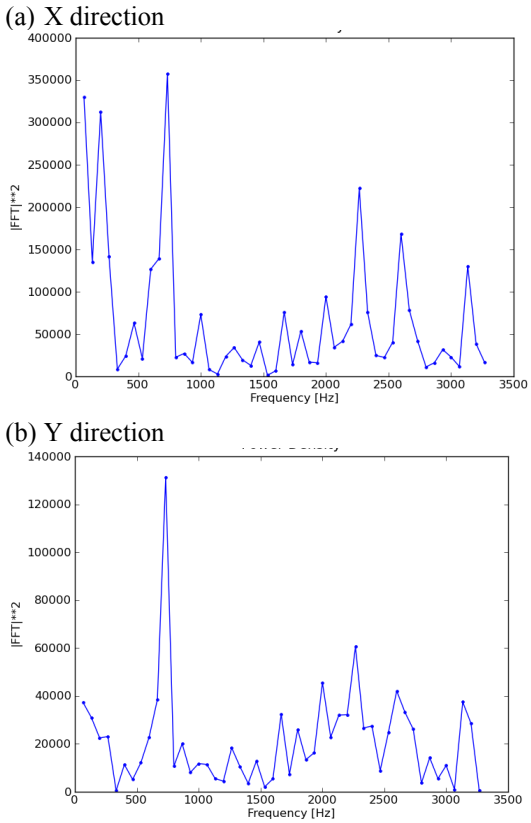

Figure 7. Periodogram of the breakpoint location fluctuation for Case 24

A major peak at the frequency of 731Hz is found in the periodograms of both x and y directions for case 24. Using Equation (1), a Strouhal number is calculated based on the jet liquid velocity and jet diameter, which is equal to 0.15. This matches well with the values indicated in the literature [7].

The same analysis can be carried out for the whole set of test cases, except for Cases 17-20, which do not have enough frames in the videos to achieve the frequency likely from FFT analysis.

Results

Instability Frequency Correlation. The instability frequencies *f* and calculated St numbers for the set of test cases, obtained by using the frequency analysis above, are listed in Table 2 .

Table 2. List of instability frequencies and St numbers

Case	*Diameter mm*	*f Hz*	We_l	*St*
1	0.5	731	117	0.15
2	0.5	1799	620	0.16
3	1.3	198	124	0.17
4	1.3	296	262	0.17
5	1.3	416	445	0.19
6	1.3	486	714	0.17
7	1.3	500	1070	0.15
8	1.3	635	1461	0.16
9	1.3	762	1911	0.17
10	1.3	365	475	0.16
11	1.3	459	749	0.16
12	1.3	508	1070	0.15
13	1.3	635	1475	0.16
14	1.3	692	1899	0.15
15	1.3	833	2400	0.16
16	1.3	896	3162	0.15
21	0.9	692	436	0.19
22	0.9	1024	1352	0.16
23	0.9	1397	3054	0.15
24	0.9	1771	4845	0.15
25	0.9	2300	8323	0.15

As shown in Table 2, the calculated St numbers for the test cases are all close to 0.15. To better validate the relationship described by Equation (1), the instability frequency *f* is plotted against the liquid jet velocity for the jet diameters 1.3mm and 0.94mm in Figure 8. A linear fitting generates the slopes for them are 0.14 and 0.12 (note that units for diameter are mm, so the coefficient should be multiplied by 0.001). Hence, the current results indicate that, for different jet diameters with similar effectively velocity ratios, the value of St can vary, as shown in Figure 8. While the values determined (0.14 and 0.12) are reasonably close to the 0.15 value, it appears that the simplified correlation shown in Equation 1 can potentially be improved upon. This development is now summarized.

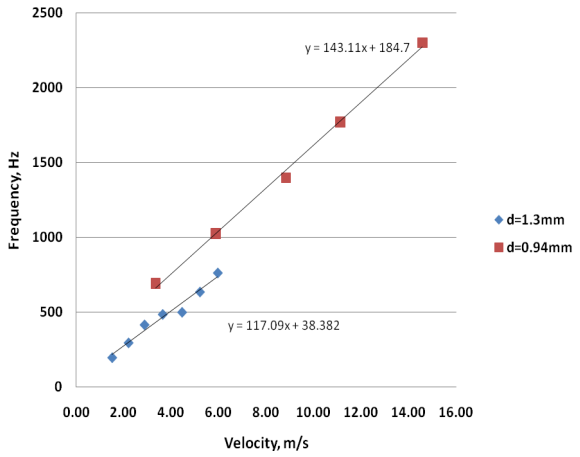

Figure 8. Frequency vs jet velocity

The first step to finding the best possible fit equation is selecting the proper independent variables. Although 25 cases is a small sample of the total possibilities in the region over which a final correlation would be applicable, each of the points is based on at least 200 images, giving a high confidence that each case is statistically significant. The pool of variables used to test for correlation was all of the pertinent non-dimensional descriptor for the experimental conditions and the orifice diameter due to its prominence in many previous studies [14,15]. These variables are: (1) aerodynamic Weber number, (2) liquid Weber number, (3) liquid column Reynolds number, (4) air Reynolds number (based on orifice diameter), and (5) the orifice diameter. Using all non-dimensional variables alleviates possible complications with units and fractional exponents later in the regression process. Ohnesorge number was not used because it differs from the Reynolds and Weber numbers only by surface tension which was not varied in the current study.

Regression Analysis. Once the variables were selected, a multivariable linear regression analysis was done based on the instability frequency and the chosen variables. First, a multivariable regression (Least Square method) was performed using the dimensionless variables aerodynamic Weber number, $We_{c,\,air}$ Reynolds number, Re_{gas}, and liquid Reynolds number, Re_{liq}.

The form of equation used for the Least Squares regression is:

$$f_{instability}[Hz] = KWe_c^{\,A}\,\mathrm{Re}_g^{\,B}\,\mathrm{Re}_l^{\,C} \qquad (10)$$

where K, A, B, and C are fitting coefficients.

The equation was linearized and the results of the Least Square fit are as follows:

$$f_{instability}[Hz] = 2.88\times10^{8}\,We_c^{\,1.96}\,\mathrm{Re}_g^{\,-3.84}\,\mathrm{Re}_l^{\,0.89} \quad (11)$$

The fitting has a R^2 value of 0.989. A comparison of the measured and predicted frequency are shown in Figure 9.

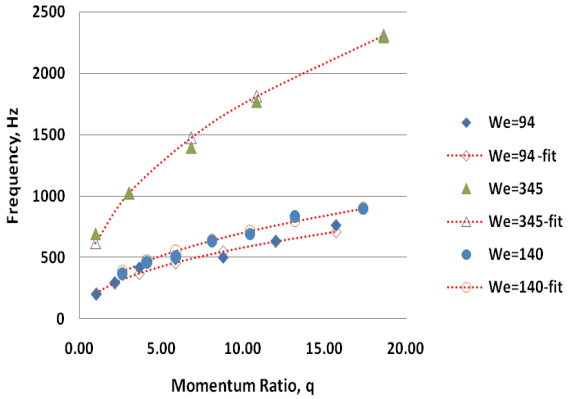

Figure 9. Plot of liquid column instability frequency.

In addition to using the nondimensional variables, a regression using the liquid Weber number, We_l, and jet diameter, d, was performed. The reason is that the instability frequency should depend mostly on liquid jet velocity and diameter, according to Equation (1).

The fit using only We_l and d shown in Figure 10 resulted in Equation (12) and has a fit R^2 value of 0.987, which indicates a very good fit.

$$f_{instability}[Hz] = 4.62\times10^{-2}\,We_l^{\,0.464}\,d_j^{\,-1.416} \quad (12)$$

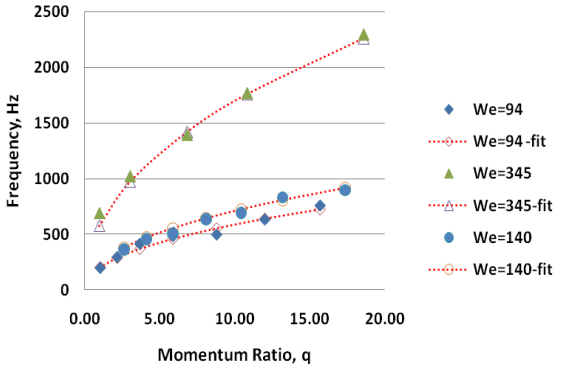

Figure 10. Comparison of measured liquid column break time and fitted values.

The results show that, with variable sets [We_c, Re_{air}, and Re_{liq}] and [We_l and d] the liquid column

break time is accurately predicted for experimental conditions in all three breakup regimes. Both Equations (11) and (12) provide a better fit of the instability frequency than Equation (1). However, by rounding the coefficients of the variables in these correlations (e.g., 1.96→2.0 in Equation 11) and applying the definition of the nondimensional variables, both equations reduce to a form that includes only jet diameter and jet velocity. In other words, they can both be simplified and reduced to the form of Equation (1) using only two independent variables: liquid jet velocity and liquid jet diameter. In may not be surprising that different values of St are obtained. Recall the value of 0.15 is consistent with the values for a rigid rod in a crossflow. In reality, the free liquid surface, circulation, and penetration into the crossflow all contribute to other subtle factors that affect the instability frequency.

Compared to Equation (11), Equation (12) uses only two variables and seems more suitable for practical applications. It also suggests that even though the liquid column breakup is a process strongly depending on both the crossflow and liquid properties, the instability frequency of the liquid column is determined only by the two important factors of liquid column. In Figure 11, the instability frequency is plotted against the liquid jet diameter and the liquid Weber number. It can be seen that the instability frequency is more sensitive to the liquid jet diameter than the liquid Weber number, which is expected according to Equation (12).

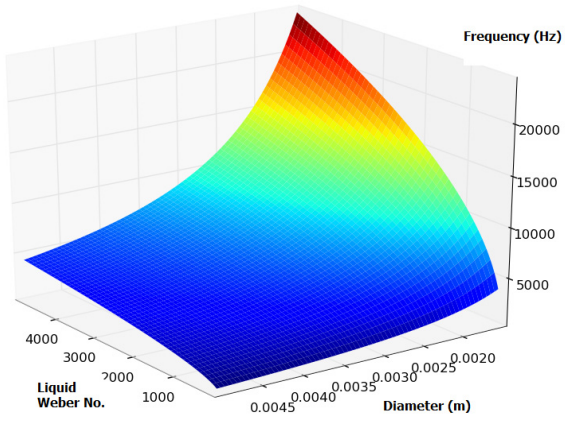

Figure 11. Instability frequency vs liquid Weber number and jet diameter

Conclusion

An automated processing methodology was used to extract liquid column break point location and liquid column trajectory from high speed video. A frequency analysis was carried out for the temporal change of the breakpoint location and the dominating frequency was obtained. Correlations were the created using data from 25 experimental cases each with over 200 data points processed by an automated program using the methodology described. The correlations developed, see equations (11) and (12), give a prediction of the liquid column instability frequency that agrees well with measurements over all three breakup regimes.

Acknowledgements

The authors gratefully acknowledge support from the U.S. Air Force (Contract FA8650-05-C-2523, Barry Kiel contract monitor) and NASA Glenn Research Center (Contract NNX09CA31C, Yolanda Hicks, contract monitor). Scott Thawley assisted in the development of the analyses codes used.

Nomenclature

d	= diameter
m	= slope (fit parameter)
y	= intercept (fit parameter)
t	= time
U, V	= velocity
ε	= error
ρ	= density
σ	= liquid surface tension
μ	= viscosity
x,y,z	= distance per sketch below
u,v,w	= velocity component per sketch below

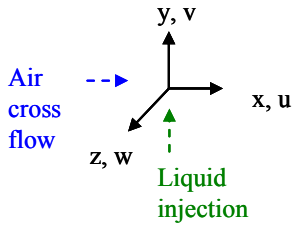

Subscripts

c	= crossflow
g	= gas
l	= liquid jet
rel	= relative velocity
o	= initial
1	= upstream
2	= downstream
Break	= breakpoint
Rel	= relative

References

1. Kush Jr. E.A., and Schetz J.A., Liquid Jet Injection into a Supersonic Flow, *AIAA Paper* 78-1180 (1975).
2. Heister S.D., Nguyen T.T., Karagonzian A.R., Modeling of Liquid jets Injected Transversely into a Supersonic Flow, *AIAA Journal* 27:422-443 (1989).

3. Brown C.T., McDonell, V.G., Near Field Behavior of a Liquid Jet in a Crossflow, *19h Annual ILASS Americas*, Toronto, Canada, May 2006
4. Madabhushi R.K., A Model For numerical Simulation of Breakup of a Liquid Jet in Crossflow, *Atomization and Sprays* 13: 413-424 (2003).
5 S.M. Thawley, U.M. Mondragon, C.T. Brown*, and V.G. McDonell, Evaluation of Column Breakpoint and Trajectory for a Plain Liquid Jet Injected into a Crossflow,ILASS Americas, 21st Annual Conference on Liquid Atomization and Spray Systems, Orlando, Florida, May 2008
6. Reitz R.D. Modeling Atomization Processes in High-pressure Vaporizing Sprays, *Atomization and Sprays*, 3:3: 309-339 (1987).
7 Moussa, Z. M., Trischka, J. W. & Eskinazi, S., The near field in the mixing of a round jet with a cross-stream. J. Fluid Mech. 80, 49-80(1977).
8 Eroglu, Adnan; Breidenthal, Robert E., Effects of periodic disturbances on structure and flame length of a jet in a crossflow, AIAA, Aerospace Sciences Meeting, 29th, Reno, NV, Jan. 7-10, 12 p(1991).
9 W. P. Jones and M. Wille, Large-eddy simulation of a plane jet in a cross-flow, Int. J. Heat and Fluid Flow 17: 296-306(1996).
10. Sallam K.A., Aalburg C., Faeth G.M., Breakup of Round Nonturbulent Liquid Jets in Gaseous Crossflow, *AIAA Journal* 42:12:2529-2540 (2004).
11 . Madabhushi, R.K., Leong, M.Y., Arienti, M., Brown, C.T., and McDonell, V.G. (2006). On the Breakup Regime Map of Liquid Jet in Crossflow, ILASS-Americas, 2006, Toronto, Canada, May.
12. Brown C.T., Mondragon U.M, McDonell V.G., Investigation of the Effect of Injector Discharge Coefficient on Penetration of a Plain Liquid Jet into a Subsonic Crossflow, *20th Annual ILASS Americas*, Chicago, Illinois, May 2007
13. Lin K.C., Kennedy P.J., and Jackson T.A., A Review on Penetration Heights of Transverse Liquid Jets in High Speed Flows, *15th Annual ILASS Americas*, Madison, Wisconsin, May 2002
14. Becker J. and Hassa C., Breakup and Atomization of a Kerosene Jet in Crossflow at Elevated Pressure, *Atomization and Sprays*, 12:1:49-63 (2002).
15. Stenzler J.M., Lee J.G., and Santavicca D.A., Penetration of Liquid Jets in a Crossflow, *AIAA Paper* No. 2003-1327 (2003)
16. Pratt W.K., *Digital Image Processing*, 2nd Edition, John Wiley & Sons, New York (1991).